Pergamon

Geochimica et Cosmochimica Acta, Vol. 66, No. 6, pp. 913–926, 2002

0016-7037/02 $22.00 + .00

PII S0016-7037(01)00827-4

Evaluation of silica-water surface chemistry using NMR spectroscopy

SUSAN A. CARROLL,[2,*] ROBERT S. MAXWELL,[1] WILLIAM BOURCIER,[2] SUE MARTIN,[2] and SUZY HULSEY[1]

[1]Chemistry and Materials Science Directorate, Lawrence Livermore National Laboratory, P.O. Box 808, Livermore, CA 94551, USA
[2]Energy and Environment Directorate, Lawrence Livermore National Laboratory, P.O. Box 808, Livermore, CA 94551, USA

(*Received January* 25, 2000; *accepted in revised form October* 1, 2001)

Abstract—We have combined traditional batch and flow-through dissolution experiments, multinuclear nuclear magnetic resonance (NMR) spectroscopy, and surface complexation modeling to re-evaluate amorphous silica reactivity as a function of solution pH and reaction affinity in NaCl and CsCl solutions. The NMR data suggest that changes in surface speciation are driven by solution pH and to a lesser extent alkali concentrations, and not by reaction time or saturation state. The ^{29}Si cross-polarization NMR results show that the concentration of silanol surface complexes decreases with increasing pH, suggesting that silanol sites polymerize to form siloxane bonds with increasing pH. Increases in silica surface charge are offset by sorption of alkali cations to ionized sites with increasing pH. It is the increase in these ionized sites that appears to control silica polymorph dissolution rates as a function of pH. The ^{23}Na and ^{133}Cs NMR results show that the alkali cations form outersphere surface complexes and that the concentration of these complexes increases with increasing pH. Changes in surface chemistry cannot explain decreases in dissolution rates as amorphous silica saturation is approached. We find no evidence for repolymerization of the silanol surface complexes to siloxane complexes at longer reaction times and constant pH. *Copyright © 2002 Elsevier Science Ltd*

1. INTRODUCTION

Significant research has been directed toward determining the reaction kinetics for the dissolution of quartz and its crystalline and amorphous polymorphs. These SiO_2 phases play critical roles in a variety of geochemical and environmental processes ranging from soil formation to disposal of radioactive waste by burial to thermally enhanced oil recovery. Laboratory studies have found that quartz and amorphous silica dissolution rates are sensitive to solution pH and alkali concentration. Dissolution rates increase by 2 to 3 orders of magnitude between pH 4 and 10 (Schwartzentruber et al., 1987; Bennett et al., 1988; Bennett, 1991; Knauss and Wollery, 1988; Wollast and Chou, 1988; Brady and Walther, 1990; House and Orr, 1992; Carroll et al., 1994; Mazer and Walther, 1994). Additionally, the pH dependence of the dissolution rate may be coupled to its dependence on dissolved alkali concentrations. Many studies have shown that dissolution rates increase with small additions of alkali cations (Bennett et al., 1988; Bennett, 1991; Dove and Crerar, 1990; Dove and Elston, 1992, Dove 1994; Berger et al., 1994). Dove and Elston (1992) and Dove (1994) relate this co-dependence of quartz dissolution on pH and sodium concentrations to increased populations of reactive deprotonated silica ($>SiO^-$) and outersphere sodium ($>SiO^-Na^+$) surface complexes. This agrees with the two-order-of-magnitude increase in the amount of surface adsorbed sodium from pH 4 to pH 10 (Allen et al., 1971). Another primary observation about silica polymorphs is that their dissolution and precipitation rates (Rimstidt and Barnes, 1980; Fleming, 1986; Renders et al., 1995; Carroll et al., 1998) are directly proportional to saturation, suggesting that the rates are microscopically reversible at the mineral-solution interface (Rimstidt and Barnes, 1980). However, the effect of saturation on surface speciation is unknown.

It is important to determine surface complexes directly, because the fundamental chemistry that controls interfacial reactions may depend on the types and concentrations of surface species. Our current understanding of silica-water surface chemistry has been derived from changes in bulk, aqueous measurements of silica gel suspensions (Bolt, 1957; Dugger, 1964; Schindler and Kamber, 1968; Tadros and Lyklema, 1969; Allen et al., 1971; Yates and Healy, 1976; Brady, 1992; Casey, 1994) and the application of various theoretical surface complexation models (Hiemstra et al., 1989; Brady, 1992; Sahai and Sverjensky, 1997). Generally, the silica-water interface consists of silanol complexes that deprotonate to form negatively charged complexes with increasing pH and increasing ionic strength. Cation sorption is also favored with increasing pH. Although, silica gel has an acid pH_{zpc} between 2 and 4, positively charged complexes from sorption of protons to silanol sites are negligible over the normal pH range.

Nuclear magnetic resonance (NMR) shows extreme promise for direct investigation of silica-water surface chemistry. Maciel and Sindorf (1980) employed surface selective cross-polarization magic-angle-spinning experiments to identify siloxane sites with four oxygen bridging atoms and silanol sites with one or two non-bridging oxygen atoms on the surface of dry silica gel. This spectroscopic technique exploits the heteronuclear dipole-dipole couplings between abundant, high-frequency ^{1}H and rare and lower frequency ^{29}Si (Pines et al., 1973; Maciel and Sindorf, 1980; Ansermet et al., 1990). As such, it can be used to identify surface species at the silica-water interface, because protons present are primarily due to chemisorption at the solid-solution interface, though some protons may be present internally (Chuang et al., 1993). Bunker et al. (1988), for example, used ^{29}Si and ^{17}O static and magic-angle-spinning NMR spectroscopy to show that stable siloxane sites polymerize from silanol sites as sodium borosilicate

* Author to whom correspondence should be addressed (carroll6@llnl.gov).

glasses dissolve in acid solutions. However in alkaline solutions, they observed a much smaller extent of surface silica polymerization.

It is also possible to directly observe alkali surface complexes with NMR spectroscopy. Kim and Kirkpatrick (1997) investigated the effects of dissolved sodium and cesium cations on the dissolution of a variety of glasses and minerals using ^{23}Na and ^{133}Cs magic-angle-spinning NMR. They were able to distinguish among sodium and cesium in the diffuse layer from those sorbed as innersphere complexes at the gel-water interface. Variable temperature studies showed that these species rapidly exchange. The samples studied were rinsed and dried at fixed humidity to control surface hydration. While beneficial for characterizing the changes in surface chemistry with the addition of monolayers of water, no specific information was gained about the speciation and motion of species in a fully hydrated surface or as a function of solution composition.

The focus of this current work is to apply ^{29}Si, ^{23}Na, and ^{133}Cs solid-state NMR methods to directly study the surface chemistry of amorphous silica as a function of solution pH and reaction time in NaCl and CsCl solutions. These NMR results are modeled within the framework of surface complexation theory and applied to silica kinetics to provide insight into silica polymorph dissolution kinetics. We present new dissolution rate data for pure SiO_2 glass as a function of pH and Na and Cs concentrations. For the NMR studies we have used silica gel as a high-surface-area surrogate for silica glass to maximize the observable signal, and have run NMR experiments on wet samples to preserve the reactive silica-water interface.

2. EXPERIMENTAL METHODS

2.1. Silica Glass Dissolution Experiments

Powdered Suprasil (Heraeus), a SiO_2 glass made by melting quartz, was used in flow-through dissolution experiments. Suprasil has an OH^- content of ~1200 ppm (0.4 mol%) and total impurities at less than 0.3 ppm (0.2 ppm iron). The glass powder was repeatedly cleaned ultrasonically with distilled and deionized water until the suspension yielded a clear supernatant after 10 min of settling, and then dried at 40°C for 24 h. The diameter of the crushed powder particles varied between 75 to 150 μm and its surface area was 0.01 m^2g^{-1} as measured by nitrogen BET. Less than 0.1% of the total mass dissolved during the experiments.

Steady-state glass dissolution rates shown in Table 1 were conducted as a function of solution pH and dissolved NaCl and CsCl at 22 and 70°C in flow-through reaction cells (described in Knauss and Wolery, 1986). The experimental data generally show steady-state dissolution after one to two days. No change in steady-state dissolution rates was found when flow rates were doubled indicating the systems behaved as true stirred reactors with no observable boundary-layer effects on dissolution. The flow rates were high (30 to 60 mL d^{-1}), such that silica concentrations were too low to cause silica saturation effects. Most silica concentrations were 10 to 1000 times below amorphous silica saturation using the data of Fournier and Rowe (1977).

2.2. Silica Gel NMR Experiments

Mallickrodt Silicar Silica Gel (100 to 200 mesh, 150Å pore diameter) was used in the nuclear magnetic resonance experiments because it provided a large reactive surface area to maximize the observable signal. The silica gel was repeatedly cleaned ultrasonically with distilled and deionized water until the suspension yielded a clear supernatant after 10 min of settling. The cleaned gel was dried at 40°C for 24 h and then stored in a plastic container at room temperature. Initial total surface area determined from a BET N_2 gas adsorption isotherm was 277 m^2g^{-1}.

The pH dependence of surface speciation tabulated in Table 2 was investigated by reacting silica gel in 0.1 molal NaCl and CsCl solutions at pH 3, 4, 5, 6, 7, 8, 9, 10, and 11. Solution pH was controlled by automatic addition of HCl, NaOH, or CsOH using a Metler DL21 autotitrator. All experiments were stirred continuously for 24 h. At the end of the experiment, an aqueous sample was filtered and analyzed by inductively coupled plasma spectroscopy for dissolved cesium, sodium, and silica; and the suspension was centrifuged, decanted, and promptly (usually within one hour) packed in rotors for ^{29}Si-NMR analysis (for about two hours). An additional amount of each sample was rinsed three times with 2 mL of deionized water to remove residual aqueous cations and also packed wet into the rotors for ^{23}Na and ^{133}Cs NMR analyses. Before the third filtration, the pH of the silica gel and deionized water mixture was measured. Sample weights were recorded after NMR analysis.

The time dependence of surface speciation was investigated by reacting silica gel in 0.1 molal NaCl and 0.01 and 0.1 molal CsCl solutions at pH 4 and 10 in batch experiments for ~1, 7, 30, and 60 d. Data are tabulated in Table 3. In the 1 and 7 d experiments, pH was controlled by automatic addition of HCl, NaOH, or CsOH using a Metler DL21 autotitrator. The longer experiments were prepared in 100% nitrogen atmosphere and in nitrogen-purged solutions to minimize pH drift, because pH was not controlled. All experiments were stirred or shaken continuously. The same sample protocol for the aqueous and NMR analyses was followed as in the pH dependent experiments, with the exception that the pH was not measured before the NMR analyses.

The ^{23}Na NMR Bloch decay analyses were run under both static and magic-angle-spinning conditions (typically $\nu_r = 3$ kHz) at 132.29 MHz on a Bruker DRX-500 spectrometer using a Bruker 4 mm cross-polarization magic-angle-spinning probe. The ^{133}Cs NMR Bloch decay analyses also were run under both static and magic-angle-spinning conditions ($\nu_r = 3$ kHz) at 65.60 MHz using the same instrument and probe. The amount of adsorbed sodium or cesium was determined by comparing the resonance area to the resonance area of an aqueous standard of known concentration of NaCl or CsCl. The weight of the sample was corrected for the amount of water in the paste by gravimetric analysis (for most samples, the content of water was ~50 wt.%).

The ^{29}Si cross-polarization NMR analyses were performed with magic-angle-spinning using spinning rates of 2 to 3 kHz at 59.5 MHz for ^{29}Si and 300.1 MHz for ^{1}H on a Chemagnetics CMX-300 spectrometer using a Chemagnetics 7.5 mm cross–polarization magic-angle-spinning probe. Typical ^{29}Si $\pi/2$ pulse lengths were 7 μs. Qualitative speciation changes in ^{29}Si cross-polarization magic-angle-spinning experiments were extracted from analyses performed using 8 ms contact times and 40 kHz proton decoupling during acquisition.

2.3. Geochemical Calculations

Solution speciation and amorphous silica saturation were calculated from the measured solution compositions at room temperature using the React (Bethke, 1994) geochemical code and the SUPCRT92 thermodynamic database (Johnson et al., 1992). Mass balance and equilibrium constants are shown in Table 4. Final pH for the month-long experiments at acid pH was calculated by adjusting H^+ to achieve charge balance in the solution. Sorption equilibria constants were calculated from the measured solution composition at room temperature using the FITEQL (Herbelin and Westall, 1999) code, the triple-layer model (Table 5), the SUPCRT92 thermodynamic data base, and the Davies equation to calculate aqueous activity coeficients.

3. RESULTS

3.1. Dissolution of Silica Glass far from Equilibrium

Figure 1 and Table 1 show the SiO_2 glass dissolution rates as a function of pH and sodium and cesium concentrations. In a similar manner to quartz (Knauss and Wolery, 1988; Brady and Walther, 1989, 1990) and silica gel (Carroll et al., 1994), silica glass dissolution rates were constant from pH 2 to 6, and

Table 1. Measured SiO_2 glass dissolution rates and initial solution composition for the flow-through dissolution experiments.

pH(T)	Rate (mol m^{-2} s^{-1})	Uncertainty ($\pm$ mol m^{-2} s^{-1})	Ionic strength (molal)	Initial solution composition
22°C NaCl				
2.04	3.3×10^{-11}	1.0×10^{-11}	0.01	0.01 m HCl, 0.01 m NaCl
4.03	2.8×10^{-11}	id	0.01	0.001 m ortho phthalic acid, HCl, 0.01 m NaCl
6.05	3.6×10^{-11}	9.6×10^{-12}	0.01	0.001 m ortho phthalic acid, HCl, 0.01 m NaCl
6.83	3.4×10^{-11}	1.9×10^{-11}	0.01	0.001 m boric acid, 0.01 m NaCl
9.22	2.7×10^{-10}	1.2×10^{-10}	0.01	0.001 m boric acid, NaOH, 0.01 m NaCl
11.97	5.0×10^{-9}	7.4×10^{-10}	0.01	0.01 m NaOH
4.02	nd		0.10	0.001 m ortho phthalic acid, HCl, 0.1 m NaCl
3.95	nd		0.94	0.001 m ortho phthalic acid, HCl, 1.0 m NaCl
9.18	4.1×10^{-10}	2.8×10^{-10}	0.10	0.001 m boric acid, NaOH, 0.1 m NaCl
8.99	1.3×10^{-9}	2.7×10^{-10}	0.94	0.001 m boric acid, NaOH, 1.0 m NaCl
22°C CsCl				
3.97	nd		0.01	0.001 m ortho phthalic acid, HCl, 0.01 m CsCl
4.05	4.7×10^{-11}	id	0.10	0.001 m ortho phthalic acid, HCl, 0.1 m CsCl
9.19	4.6×10^{-10}	3.4×10^{-10}	0.01	0.001 m boric acid, NaOH, 0.01 m CsCl
9.22	3.6×10^{-10}	3.0×10^{-10}	0.10	0.001 m boric acid, NaOH, 0.1 m CsCl
70°C NaCl				
2.03	8.8×10^{-11}	3.1×10^{-11}	0.01	0.01 m HCl, 0.01 m NaCl
4.07	6.9×10^{-11}	1.7×10^{-11}	0.01	0.001 m ortho phthalic acid, HCl, 0.01 m NaCl
5.90	9.9×10^{-11}	1.1×10^{-10}	0.01	0.001 m ortho phthalic acid, HCl, 0.01 m NaCl
6.72	5.6×10^{-10}	1.2×10^{-10}	0.01	0.001 m boric acid, 0.01 m NaCl
8.67	1.4×10^{-8}	1.6×10^{-9}	0.01	0.001 m boric acid, NaOH, 0.01 m NaCl
10.51	1.7×10^{-7}	2.2×10^{-8}	0.01	0.01 m NaOH
4.01	1.0×10^{-10}	1.5×10^{-11}	0.10	0.001 m ortho phthalic acid, HCl, 0.1 m NaCl
3.97	3.3×10^{-10}	3.5×10^{-11}	0.94	0.001 m ortho phthalic acid, HCl, 1.0 m NaCl
8.55	2.0×10^{-8}	5.7×10^{-9}	0.10	0.001 m boric acid, NaOH, 0.1 m NaCl
8.33	1.5×10^{-8}	5.6×10^{-9}	0.94	0.001 m boric acid, NaOH, 1.0 m NaCl
70°C CsCl				
3.94	1.3×10^{-10}	1.6×10^{-11}	0.01	0.001 m ortho phthalic acid, HCl, 0.01 m CsCl
4.05	1.6×10^{-10}	4.9×10^{-11}	0.10	0.001 m ortho phthalic acid, HCl, 0.1 m CsCl
8.53	1.4×10^{-8}	2.9×10^{-9}	0.01	0.001 m boric acid, NaOH, 0.01 m CsCl
8.53	3.4×10^{-9}	6.4×10^{-10}	0.10	0.001 m boric acid, NaOH, 0.1 m CsCl

id = insufficient data to calculate uncertainty.
nd = silica concentration below detection limit.

increased by 100 times at 22°C and 1000 times at 70°C from pH 6 to 12. These results also agree with pH trends for SiO_2 glass dissolution rates reported in previous studies (Mazer and Walther, 1994; Wirth and Gieskes, 1979). We can adaquately describe SiO_2 dissolution rates far from equilibrium as a function of pH and temperature using the following equation:

$$Rate(mol\ m^{-2}\ s^{-1}) = 10^{k_1}\ 10^{(-E_{a,1}/2.303\,RT)} + 10^{k_2}10^{(-E_{a,2}/2.303\,RT)} \quad (1)$$

where the universal gas constant, $R = 8.314 \times 10^{-3}$ (mol KJ^{-1}); temperature, T is in Kelvin; $k_1 = -5.72$ (mol $m^{-2}s^{-1}$) and $E_{a,1} = 26.9$ (KJ mol^{-1}) and the pH dependence of k_2 (mol $m^{-2}s^{-1}$) and $E_{a,2}$ (KJ mol^{-1}) equal:

$$k_2 = -13.7 + 1.91 \times pH \quad (2)$$

$$E_{a,2} = 8.15 \times pH \quad (3)$$

Rate constants and activation energies were derived from Arrhenius plots of log rate vs pH at 22 and 70°C for rates at pH < 7 (subscript 1) where the rates are independent of pH and pH > 7 (subscript 2) where the rates are dependent on pH. The error bars shown in Figure 1 reflect the uncertainty of a single steady-state dissolution rate as measured by the dissolved silica concentrations as a function of time.

The effect of alkali concentration on SiO_2 glass dissolution rates is not consistent as a function of pH or temperature and may reflect experimental uncertainty (Fig. 1). An increase in sodium concentration from 0.01 to 1 molal enhanced dissolution rates by 5 times at about pH 9 (22°C) and pH 4 (70°C), but showed no measurable effect on dissolution rates at about pH 8 (70°C). An increase in cesium concentration from 0.01 to 0.1 molal showed no measurable effect on dissolution rates at about pH 9 (25°C) and pH 4 (70°C), but appeared to decrease the dissolution rate by 5 times at about pH 8 (70°C).

3.2. Dissolution of Silica Gel near Equilibrium

Results of the macroscopic dissolution of silica gel in 0.1 molal NaCl and 0.01 and 0.1 molal CsCl solutions are represented in Figure 2. The plot shows the total dissolved silica

Table 2. Solution and surface chemistry of silica gel as a function of solution pH.

Expt. No.	pH	g/L	$Na_{initial}$ molal	$Cl_{initial}$ molal	Na_{final} molal	±	Si_{final} molal	±
Si 75	2.79	20.37	0.097	0.098				
Si 74	3.36	21.61	0.098	0.098				
Si 76	4.00	19.92	0.091	0.092				
Si 65	3.96	19.99	0.100	0.101	0.101	0.001	4.7×10^{-4}	6.5×10^{-6}
Si 67	4.94	20.08	0.100	0.101	0.101	0.001	7.6×10^{-4}	6.0×10^{-6}
Si 69	5.97	19.98	0.100	0.101	0.099	0.001	1.0×10^{-3}	1.7×10^{-5}
Si 63	7.03	20.05	0.101	0.100	0.095	0.001	2.0×10^{-3}	3.0×10^{-5}
Si 64	8.00	19.73	0.101	0.098	0.098	0.001	2.2×10^{-3}	2.6×10^{-5}
Si 66	9.00	19.11	0.100	0.095	0.098	0.001	2.4×10^{-3}	1.3×10^{-5}
Si 61	10.00	17.27	0.100	0.086	0.094	0.001	6.2×10^{-3}	3.2×10^{-6}
Si 68	11.00	19.41	0.132	0.096	0.122	0.001	2.6×10^{-2}	3.7×10^{-4}

Expt. No.	^{1}>SiOH mol m^{-2} (ave NMR)	±	$^{2}Na_{sorbed}$ mol m^{-2} (ΔNa_{aq})	±	$^{3}\sigma \times F^{-2}$ mol m^{-2}	±	^{4}pH (Na NMR)	$^{4}Na_{sorbed}$ mol m^{-2} (Na NMR)
Si 75	7.9×10^{-6}	7×10^{-7}			-0.5×10^{-7}	6×10^{-8}		
Si 74	7.9×10^{-6}	7×10^{-7}			0.5×10^{-7}	6×10^{-8}		
Si 76	7.9×10^{-6}	7×10^{-7}			1.2×10^{-7}	6×10^{-8}		
Si 65	7.9×10^{-6}	7×10^{-7}	-0.2×10^{-6}	0.7×10^{-7}	1.2×10^{-7}	6×10^{-8}	5.6	0.2×10^{-7}
Si 67	5.7×10^{-6}	13×10^{-7}	-0.1×10^{-6}	1.5×10^{-7}	0.7×10^{-7}	6×10^{-8}	7.0	0.4×10^{-7}
Si 69	3.6×10^{-6}	5×10^{-7}	0.3×10^{-6}	1.8×10^{-7}	0.5×10^{-7}	6×10^{-8}	7.3	0.9×10^{-7}
Si 63	2.0×10^{-6}	9×10^{-7}	1.0×10^{-6}	3.8×10^{-7}	-0.7×10^{-7}	6×10^{-8}	8.8	2.2×10^{-7}
Si 64	1.7×10^{-6}	6×10^{-7}	0.5×10^{-6}	4.8×10^{-7}	-3.6×10^{-7}	6×10^{-8}	9.6	2.8×10^{-7}
Si 66	0.8×10^{-6}	3×10^{-7}	0.5×10^{-6}	2.1×10^{-7}	-7.5×10^{-7}	6×10^{-8}	10.0	5.4×10^{-7}
Si 61	1.6×10^{-6}	1×10^{-7}	1.2×10^{-6}	1.7×10^{-7}	-2.0×10^{-6}	6×10^{-8}	10.6	10.0×10^{-7}
Si 68	0.4×10^{-6}	1×10^{-7}	1.8×10^{-6}	2.6×10^{-7}	-1.6×10^{-6}	6×10^{-8}	11.0	8.8×10^{-7}

Expt. No.	pH	g/L	$Cs_{initial}$ molal	$Cl_{initial}$ molal	Cs_{final} molal	±	Si_{final} molal	±
Si 56	3.97	19.87	0.102	0.103	0.103	0.001	2.9×10^{-4}	0.6×10^{-5}
Si 55	4.98	19.97	0.103	0.103	0.102	0.001	6.6×10^{-4}	1.8×10^{-5}
Si 54	6.00	20.04	0.103	0.103	0.103	0.001	9.1×10^{-4}	1.5×10^{-5}
Si 57	6.97	20.15	0.103	0.103	0.104	0.002	1.1×10^{-3}	0.6×10^{-5}
Si 58	8.07	19.98	0.103	0.102	0.103	0.001	1.3×10^{-3}	2.2×10^{-5}
Si 59	9.02	19.53	0.103	0.101	0.103	0.001	1.4×10^{-3}	1.2×10^{-5}
Si 60	10.02	18.89	0.103	0.097	0.100	0.001	2.2×10^{-3}	3.1×10^{-5}
Si 62	11.01	17.14	0.103	0.088	0.099	0.002	6.5×10^{-3}	9.7×10^{-5}

Expt. No.	^{1}>SiOH mol m^{-2} (ave NMR)	±	$^{2}Cs_{sorbed}$ mol m^{-2} (ΔCs_{aq})	±	$^{3}\sigma \times F^{-2}$ mol m^{-2}	±	^{4}pH (Cs NMR)	$^{4}Cs_{sorbed}$ mol m^{-2} (Cs NMR)
Si 56	7.9×10^{-6}	7×10^{-7}	-0.2×10^{-7}	3.4×10^{-7}	1.4×10^{-7}	4×10^{-8}	5.6	0.7×10^{-7}
Si 55	5.7×10^{-6}	13×10^{-7}	0.7×10^{-7}	4.0×10^{-7}	1.0×10^{-7}	4×10^{-8}	7.3	1.2×10^{-7}
Si 54	3.6×10^{-6}	5×10^{-7}	-0.5×10^{-7}	3.3×10^{-7}	0.6×10^{-7}	4×10^{-8}	7.9	3.3×10^{-7}
Si 57	2.0×10^{-6}	9×10^{-7}	-0.5×10^{-7}	5.4×10^{-7}	0.0×10^{-7}	4×10^{-8}	8.1	4.2×10^{-7}
Si 58	1.7×10^{-6}	6×10^{-7}	0.8×10^{-7}	2.6×10^{-7}	-1.8×10^{-7}	4×10^{-8}	8.4	9.8×10^{-7}
Si 59	0.8×10^{-6}	3×10^{-7}	1.3×10^{-7}	4.3×10^{-7}	-3.6×10^{-7}	4×10^{-8}	9.7	1.9×10^{-6}
Si 60	1.6×10^{-6}	1×10^{-7}	5.2×10^{-7}	2.9×10^{-7}	-7.7×10^{-7}	4×10^{-8}	10.2	2.7×10^{-6}
Si 62	0.4×10^{-6}	1×10^{-7}	6.6×10^{-7}	7.5×10^{-7}	-1.4×10^{-6}	4×10^{-8}	10.5	4.1×10^{-6}

[1] Average >SiOH concentration and standard deviation from the NaCl and CsCl experiments.
[2] Na_{sorbed} and Cs_{sorbed} calculated as the difference between the initial and final dissolved Na or Cs concentrations. Uncertainty is calculated as twice analytical standard deviation of the final aqueous alkali concentrations.
[3] $\sigma \times F^{-1}$ was calculated from acid-base chemistry and uncertainty was estimated as the standard deviation below pH 6.
[4] Na_{sorbed} and Cs_{sorbed} and pH of the silica gel after it was rinsed with 6 ml of distilled and de-ionized water.

versus time and the amorphous silica saturation index versus time. The amorphous silica saturation state is represented by the saturation index ($SI = Q/K$), where K is the solubility constant for amorphous silica, Q is the activity quotient ($a^{SiO_{2(aq)}}/a^{SiO_{2(s)}}$), and $a^{SiO_{2(s)}}$ is assumed to be equal to unity. At pH 4, the amount of dissolved silica was observed to increase as a function of time and approached an asymptopic limit at 30 to 60 d as the solution approached saturation with amorphous silica. At pH 10, however, the amount of dissolved silica increased in the first few days but was much lower at 30 and 60 d. The lower silica concentration at 30 and 60 d reflected the neutralization of the unbuffered solution as silica gel dissolved. A duplicate experiment showed that the solution pH drifted from pH 10.0 to 8.6 in CsCl solutions and from pH 10.0 to 9.0

Table 3. Time dependence of silica-water surface speciation. Solution composition and percent ^{29}Si cross-polarization NMR resonance at pH 4 and 10 in 0.1 molal NaCl and CsCl solutions.

Experiment No.	Days	pH	Na or Cs molal	Cl molal	Si molal	±	Amorphous silica saturation index	^{29}Si NMR Q_2 (%)	Q_3 (%)	Q_4 (%)
pH 4, 0.1 M NaCl										
35A	0.96	4	0.097	0.098	2.3×10^{-4}	1.6×10^{-6}	−0.93	5.9	60.3	33.8
36A	6.98	4	0.097	0.098	4.8×10^{-4}	6.1×10^{-6}	−0.61	5.9	60.3	33.8
37A	33.10	3.5[1]	0.098	0.098	1.1×10^{-3}	1.2×10^{-5}	−0.24	7.4	60.5	32.1
21	54.92	2.9[1]	0.098	0.098	1.6×10^{-3}	1.8×10^{-4}	−0.08 (+0.05/−0.04)			
pH 10, 0.1 M NaCl										
38A	0.97	10	0.098	0.089	3.7×10^{-3}	6.4×10^{-5}	−0.50	0.4	40.1	59.4
1	6.01	10	0.098	0.086	5.6×10^{-3}	3.4×10^{-4}	−0.31 (+0.03/−0.02)			
39A	7.03	10	0.098	0.080	4.8×10^{-3}	4.8×10^{-5}	−0.36	2.2	40.1	57.7
2	32.90	9.0[2]	0.098	0.094	2.7×10^{-3}	5.5×10^{-5}	−0.04 (+0.11/−0.24)			
40a	34.93	9.0[2]	0.098	0.095	2.2×10^{-3}	3.4×10^{-5}	−0.13 (+0.11/−0.24)	0.0	48.0	52.0
pH4, 0.01 M CsCl										
13	1.02	4	0.010	0.010	2.9×10^{-4}	5.6×10^{-6}	−0.83			
25	7.00	4	0.010	0.011	9.5×10^{-4}	1.0×10^{-6}	−0.31			
14	56.79	3.7[1]	0.010	0.010	1.7×10^{-3}	1.0×10^{-5}	−0.05			
pH 10, 0.01 M CsCl										
12	1.06	10	0.016	0.009	2.4×10^{-3}	2.6×10^{-5}	−0.18			
24	6.94	10	0.023	0.009	2.9×10^{-3}	2.7×10^{-5}	−0.18			
15	56.79	8.6[2]	0.011	0.010	2.4×10^{-3}	1.4×10^{-5}	0.07 (+0.01/−0.04)			
pH 4, 0.1 M CsCl										
29A	1.00	4	0.097	0.098	3.1×10^{-4}	6.0×10^{-6}	−0.78	4.2	60.2	35.5
18	1.03	4	0.097	0.098	3.9×10^{-4}	1.0×10^{-6}	−0.69			
23	6.94	4	0.097	0.098	7.6×10^{-4}	3.9×10^{-6}	−0.41			
30A	7.08	4	0.097	0.098	1.1×10^{-3}	1.4×10^{-5}	−0.26	9.9	58.6	31.3
31A	33.90	3.2[1]	0.097	0.098	1.4×10^{-3}	1.0×10^{-5}	−0.14	9.9	58.6	31.3
16	54.92	3.5[1]	0.098	0.098	1.8×10^{-3}	3.0×10^{-5}	−0.02			
pH 10, 0.1 M CsCl										
32A	0.98	10	0.098	0.088	3.3×10^{-3}	1.6×10^{-5}	−0.16	1.1	39.4	59.5
19	1.00	10	0.098	0.092	2.5×10^{-3}	1.4×10^{-5}	−0.29			
33A	6.75	10	0.098	0.081	3.2×10^{-3}	4.7×10^{-5}	−0.14	6.7	46.9	46.4
20	7.00	10	0.098	0.082	5.0×10^{-3}	2.0×10^{-5}	−0.01			
34	36.89	8.6[2]	0.098	0.094	2.7×10^{-3}	5.8×10^{-5}	0.13 (+0.01/−0.05)	0.5	40.5	59.0
17	56.79	8.6[2]	0.098	0.097	2.1×10^{-3}	8.5×10^{-6}	0.02 (+0.01/−0.05)			

[1] pH calculated by charge balance.
[2] pH equal to measured experiment, uncertainty in saturation index is calculated from measured Si at ±0.5 pH.

Table 4. Thermodynamic data (Johnson et al., 1992).

	log K (25°C)
$Cs^+ + Cl^- = CsCl(aq)$	−0.14
$Na^+ + Cl^- = NaCl(aq)$	−0.78
$Cs^+ + H_2O = CsOH(aq) + H^+$	−15.68
$Na^+ + H_2O = NaOH(aq) + H^+$	−14.79
SiO_2 (quartz) = $SiO_2(aq)$	−4.0
SiO_2 (am. si.) = SiO_2 (aq)	−2.71
SiO_2 (aq) + $H_2O = HSiO_3^- + H^+$	−9.95
SiO_2 (aq) + $Na^+ + H_2O = NaHSiO_3(aq) + H^+$	−8.30

in NaCl solutions. At these pH values, the solutions were near amorphous silica saturation, whereas solutions from the 1 and 7 d experiments at pH 10 were undersaturated with respect to amorphous silica, as shown in Figure 2. Uncertainty in the saturation index was calculated at ± 0.5 pH for the alkaline experiments reacted for 30 and 60 d, because the final pH of each experiment was not measured. With the exception of two experiments (1 and 21), uncertainty due to dissolved silica analytical standard deviation is smaller than the size of the symbols in Figure 2.

3.3. Silica-Water Surface Chemistry

In this section we show two types of data that will be used as the basis for the interpretation of the silica-water surface chem-

Table 5. Triple Layer Surface Complexation Model (Yates et al., 1974; Davis et al., 1978) used to calculate Cs and Na sorption to amorphous silica. { } indicates the activity of aqueous species, [ ] indicates the concentration of surface species, σ and ψ are the respective charge and electric potential for the O-plane (o), the β-plane (β) and the diffuse plane (d), C_1 is the inner layer capacitance and C_2 is the is the outer layer capacitance, ε_o is the permittivity of a vacuum, ε_w is the permittivity of water, F = 96,485 C mol^{-1}, R = 8.314 $\times$ 10^{-3} KJ mol^{-1} K^{-1}, and T 298 K.

	Log K_{intr}
1. $>\text{SiOH} \Leftrightarrow > \text{SiO}^- + \text{H}^+$ $K_{>SiO^-} = \frac{[>\text{SiO}^-]\{\text{H}^+\}}{[>\text{SiOH}]} 10^{-(\text{F}\psi_0/2.303\text{RT})}$	-7.5 ± 1.0
2a. $>\text{SiOH} + \text{Cs}^+ \Leftrightarrow > \text{SiO}^-\text{Cs}^+ + \text{H}^+$ $K_{>\text{SiO}^-\text{Cs}^+} = \frac{[>\text{SiO}^-\text{Cs}^+]\{\text{H}^+\}}{[>\text{SiOH}]\{\text{Cs}^+\}} 10^{((\psi_\beta - \psi_o)\text{F}/2.303\text{RT})}$	-7.8 ± 0.1 $C_1 = 1(\text{Fm}^{-2})$ $C_2 = 0.2(\text{Fm}^{-2})$
2b. $>\text{SiOH} + \text{Na}^+ \Leftrightarrow > \text{SiO}^-\text{Na}^+ + \text{H}^+$ $K_{>SiO\ Na^+} = \frac{[>\text{SiO}^-\text{Na}^+]\{\text{H}^+\}}{[>\text{SiOH}]\{\text{Na}^+\}} 10^{((\psi_\beta - \psi_o)\text{F}/2.303\text{RT})}$	-6.5 ± 0.4 $C_1 = 1\ (\text{Fm}^{-2})$ $C_2 = 0.2\ (\text{Fm}^{-2})$
3. $\sigma_0 = C_1(\psi_0 - \psi_\beta)$	
4. $\sigma_d = C_2(\psi_d - \psi_\beta)$	
5a. $\sigma_o = \frac{F}{A}(-[>\text{SiO}^-] - [>\text{SiO}^-\text{Cs}^+])$	
5b. $\sigma_o = \frac{F}{A}(-[>\text{SiO}^-] - [>\text{SiO}^-\text{Na}^+])$	
6a. $\sigma_\beta = \frac{F}{A}[>\text{SiO}^-\text{Cs}^+]$	
6b. $\sigma_\beta = \frac{F}{A}[>\text{SiO}^-\text{Na}^+]$	
7. $\sigma_d = \sqrt{8\varepsilon_0\varepsilon_w\text{RTI}} \sinh\left(\frac{F\psi_d}{2\text{RT}}\right) \mu\text{C/cm}^2$	
8. $\sigma_0 + \sigma_\beta + \sigma_d = 0$	
9a. $[>\text{SiOH}]_{T,pH} = ([>\text{SiOH}] + [>\text{SiO}^-] + [>\text{SiO}^-\text{Cs}^+])$	
9b. $[>\text{SiOH}]_{T,pH} = ([>\text{SiOH}] + [>\text{SiO}^-] + [>\text{SiO}^-\text{Na}^+])$	

istry as a function of solution composition. One data set is direct measure of silanol and alkali surface complexes on the silica gel suspension using NMR spectroscopy. The other data set is a measure of surface charge and alkali sorption calculated from changes in the bulk solution. Comparison of these data sets yields three important findings.

1. Surface charge cannot account for strong pH-dependence of silanol surface complexes observed in the NMR spectra.
2. Surface charge appears to be compensated by outersphere sorption of alkali ions.
3. At constant pH, the concentration of silanol surface complexes is independent of solution saturation.

3.3.1. ^{23}Na and ^{133}Cs NMR studies of cation adsorption

Figure 3 shows the solid-state ^{23}Na and ^{133}Cs magic-angle-spinning NMR spectra at room temperature of silica gel samples reacted in 0.1 molal NaCl and CsCl from pH 4 to 11 for 24 h. We use this data to establish pH trends for alkali sorption and to identify the local structure of the sorbed complex. We do not use it to quantify surface complexation reactions, because the ionic strenth was reduced when the suspensions were rinsed to separate the sorbed and aqueous alkali signals. The spectra are composed of a single relatively narrow resonance with no associated spinning sidebands and with the same chemical shift as aqueous NaCl or CsCl. The intensity of both the ^{23}Na and ^{133}Cs resonances steadily increased with increased pH. The detected NMR signal survived up to 10 separate wash/filter cycles with no change in amount of adsorbed cation, suggesting that the signal represents alkali sorption on the silica surface and not dissolved alkali in solution. The concentration of sodium and cesium sorbed to the rinsed silica gel surfaces was measured against the areas of ^{23}Na and ^{133}Cs resonances from standard solutions (Table 2). The ^{23}Na and ^{133}Cs solid-state NMR results provide direct, spectroscopic evidence that sodium and cesium sorb preferentially at high pH by 20 to 40 times higher than at low pH. In a similar manner to the ^{29}Si spectra (see below), no differences in cation concentration were observed with reaction time, suggesting sorption rapidly reaches equilibrium (data not shown).

Sodium and cesium cations likely form mobile outersphere surface complexes at the silica-water surface based on the narrow linewidth of the spectra, the lack of chemical shift from aqueous sodium and cesium, and negligible quadrupolar couplings. Both the ^{23}Na and ^{133}Cs resonances narrow slightly with slow spinning ($\nu_r > 500$ Hz) compared with spectra recorded under static conditions. Other than this, we observed no significant changes in lineshape or width with further increases in spinning speed and no significant spinning sidebands in samples spun faster than 500 Hz. Nutation experiments also showed no detectable amount of ^{23}Na or ^{133}Cs with large quadrupolar interactions (i.e., for all samples, the $\pi/2$ pulse length was equivalent to the $\pi/2$ pulse length of the standard solution). These data are consistent with cations that are undergoing motional dynamics on a fast timescale (a motional correlation time, τ_c, $< 10^{-6}$ s) (Abragam, 1961). For compar-

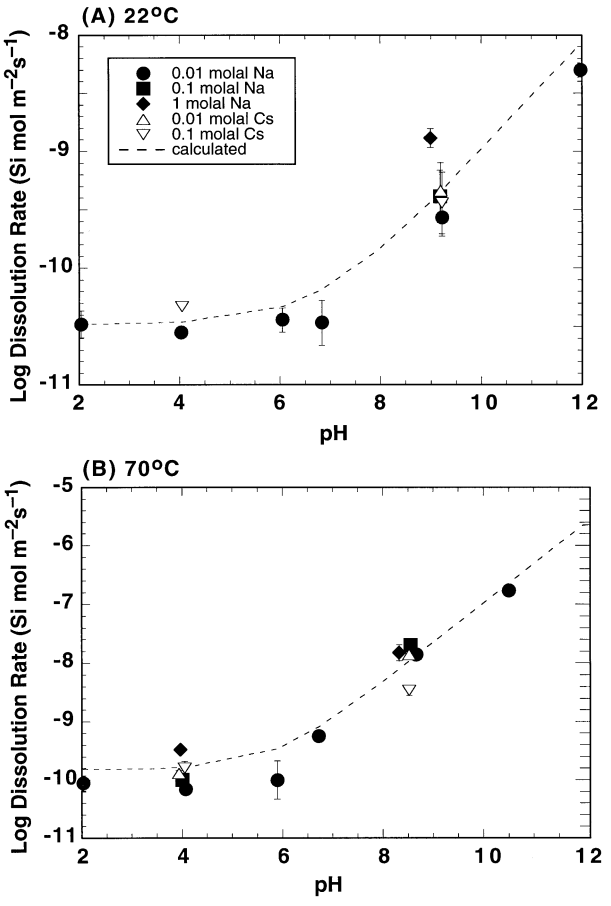

Fig. 1. SiO_2 glass dissolution rates in CsCl and NaCl solutions at 22°C (A) and 70°C (B) plotted as log dissolution rate Si mol m^{-2} s^{-1} versus pH. Dissolution rates and solution compositions are listed in Table 1. The dashed lines represent rates calculated from the overall rate expression (Eqn. 1).

ison, motionally constrained sodium or cesium in oxide solids have relatively large quadrupolar coupling and/or chemical shift anisotropy parameters.

We were unable to reproduce the ^{23}Na and ^{133}Cs NMR results of Kim and Kirkpatric (1997), who observed multiple cation sites by magic-angle-spinning NMR methods. In their study, they carefully controlled the hydration of the silica surface after reaction by first rinsing and then drying their gel surfaces in controlled-humidity atmospheres. The goal of their approach was to investigate both surface cation sorption sites and sorption dynamics. However, questions arise as to the changes induced by their equilibration step. We chose to look at the cation NMR by simply rinsing away the abundant aqueous phase and observing the wet surface layer.

3.3.2. ^{29}Si-NMR studies

Figure 4 shows ^{29}Si cross-polarization magic-angle-spinning spectra for silica gel reacted in aqueous solutions from pH 4 to 11 in the presence of 0.1 molal CsCl and NaCl solutions. As can be seen in these figures, solution pH strongly affected the silica-water surface chemistry, where the intensity of the ^{29}Si spectra decreased with increasing pH. However, at constant pH, silica-water surface chemistry did not change with time and approach to saturation as shown in Figure 5. The ^{29}Si cross-polarization NMR spectra shown in Figure 4 are characterized by three broad resonances assigned to silanol sites with three bridging oxygen atoms at -100 ppm resonance (Q_3), silanol sites with two bridging oxygen sites at -90 ppm resonance (Q_2), and siloxane sites with four bridging oxygen atoms at -110 ppm (Q_4). In general, the cross-polarization spectra are dominated by the Q_3 resonance, in contrast with bulk structure speciation. This is expected, because the cross-polarization experiment selectively enhances ^{29}Si signals in proximity to protons. The residual Q_4 sites are observed due to long range dipolar couplings to neighboring Q_2 and Q_3 species. The spectra shown here are similar to spectra reported for calcined silica gels (Maciel and Sindrof, 1980). We do not detect any small chemical shifts due to complexation with Cs and Na as reported for small silica oligomers in solution (Kinrade and Swaddle, 1988; Wijnen et al., 1990). This is because the resonances of amorphous silica are broadened by large distributions of chemical shifts from perturbations of the SiO_4 tetrahedra.

The decrease in the ^{29}Si cross-polarization NMR spectra as a function of pH can be explained by either a change in the speciation at the silica-water interface or a change in the ^{1}H-^{29}Si spin system parameters due to structural or motional changes. Because heteronuclear dipolar couplings between ^{1}H and ^{29}Si in cross-polarization spectra are a function of internuclear distances and motional timescales, changes in the coupling parameters can be revealed through study of the dependence of the spectral intensities upon cross-polarization contact time (Pines et al., 1973). Figure 6 plots the spectral intensity for the Q_3 and Q_4 species as a function of contact time for pH 4 and pH 10 samples. The cross-polarization dynamics are identical within experimental error and, therefore, we assign the differences in cross-polarization spectra to proton speciation changes at the silica-water interface.

In general, quantitative speciation is difficult to obtain from cross-polarization experiments, because a number of parameters must be independently determined (Pines et al., 1973; Maciel and Sindorf, 1980). Previous methods have been developed to directly measure silanol speciation on silica surfaces by high-resolution ^{1}H solid-state NMR methods on carefully dehydrated samples (Bronnimann et al., 1988; Chuang and Maciel, 1993; Changhua and Maciel, 1996). It is not possible to directly measure the site density by ^{1}H-NMR in our study because large amounts of water would mask the signal. However, cross-polarization spectra are a reasonable measure of the number of silanol sites if correct calibrations are employed, because the ^{29}Si cross-polarization NMR spectrum arises from ^{29}Si species coupled to relatively immobile protons. The basis of our calibration is that the gaussian fits to the silanol signal ($2Q_2 + Q_3$) at pH $\leq$ 4 are proportional to total surface site density and any bulk silanol sites that are inaccessible to water. This is a reasonable assumption, because the intensity of the spectra at pH $\leq$ 4 is constant within experimental uncertainty. We use a surface site density of 4.6 (site nm^{-2}) determined by isotopic vapor exchange on dry silica gel (Zhuravlev and Kiselev, 1962; Davydov et al., 1964; Madeley and Richmond, 1972). This site density is similar to values reported for tritium exchange in suspensions containing gel that was dehydrated at

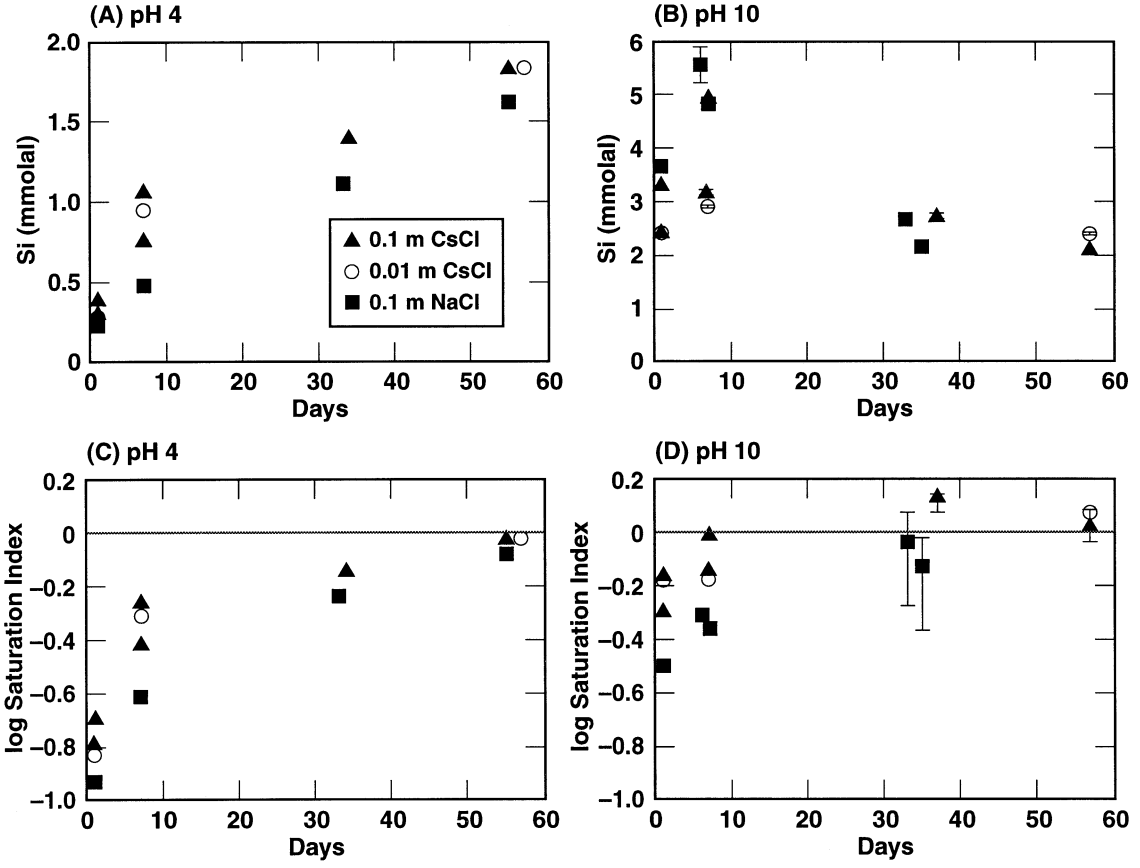

Fig. 2. Dissolution of silica gel as a function of time at pH 4 and pH 10 shown as dissolved silica (A, B) and with respect to amorphous silica saturation (C, D) in 0.1-molal CsCl solutions (solid triangles), 0.01-molal CsCl (open circles), and 0.1-molal NaCl (solid squares). In B and D, the pH was estimated to be 8.6 in CsCl solutions and 9.0 in NaCl solutions for 30-d and longer experiments (see Table 3 and "Dissolution of Silica Gel Near Equilibrium").

elevated temperatures during its synthesis (Yates and Healy, 1976), as was the gel used in our study. We correct the spectra for inaccessible silanol sites using a value that is 9.3% of the silanol intensity at pH $\leq$ 4. This is the proportion of inaccessible silanol sites determined by deuterium-exchange experiments (Chuang et al., 1993). This correction is applied equally as a function of pH, because the number of inaccessible silanol sites should be constant. The concentration of surface silanol sites is then calculated from the total site density and the change in corrected spectra intensity as a function of pH, and reported as the average values determined in the CsCl and NaCl experiments in Figure 7 and Table 2. The concentration of silanol sites dramatically decreases from 100% of the surface site density at pH 4 to less than 10% of the surface site density at pH 11, indicating that most of the surface sites are available for surface complexation reactions. This is an important observation, because previous studies of surface chemistry derived from potentiometric titration of a wide variety of oxide suspensions indicate that only a fraction of surface sites are reactive (see compilation and evaluation of experimental data in Sahai and Sverjensky, 1997). As we discussed above, the observed pH-dependence of silanol sites is not an artifact of cross-polarization dynamics. Nor is it likely to be an artifact of the experimental protocol because the 24 h pH-stat experiments exhibited equilibrium behavior. Any changes in suspension chemistry during the hour between the end of the pH-stat experiment and the NMR analyses would be minimal. Additionally, the silica gel pastes that were packed into the NMR rotors contained $\sim$ 50 wt. % water and did not evaporate during 2 h NMR analyses.

3.3.3. Surface charge and alkali sorption

Figure 7 shows the surface charge and alkali sorption for silica gel reacted in aqueous solutions from pH 3 to 11 in the presence of 0.1 molal CsCl and NaCl. The complementary NMR spectra are shown in Figures 3 and 4. Our calculations of silica surface charge from changes in the solution composition are similar to the results of other studies, in which the surface is neutral from pH 3 to 7 and becomes increasingly more negative above pH 7 or 8 (Bolt, 1957; Schindler and Kamber, 1968; Yates and Healy, 1976; Brady, 1992; Casey, 1994). We calculate the surface charge, σ, from the 24 h pH-stat experiments as the difference between added and measured H^+ and OH^- concentrations corrected for hydrolysis associated with aqueous speciation:

$$\sigma(\mathrm{C\ m^{-2}}) = \frac{F}{A}\left([\mathrm{H^+}]_{\mathrm{add}} - [\mathrm{H^+}]_{\mathrm{meas}} - [\mathrm{OH^-}]_{\mathrm{add}} + [\mathrm{OH^-}]_{\mathrm{meas}} - [\mathrm{H_3SiO_4^-}] - [\mathrm{MH_3SiO_4(aq)}] - [\mathrm{MOH}]\right) \quad (4)$$

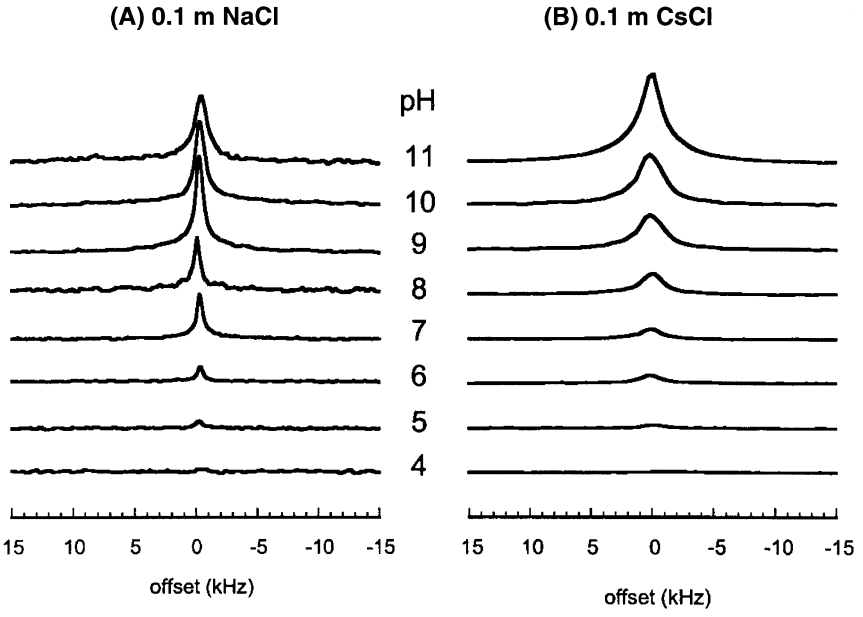

Fig. 3. The pH dependence of ^{23}Na and ^{133}Cs magic-angle-spinning NMR spectra of amorphous silica reacted in 0.1-molal NaCl (A) and CsCl (B) at 25°C. The intensities of the spectra have been normalized by weight and plotted relative to the same vertical scale.

where A is the surface area, F is the Faraday constant, and M refers to Cs or Na. Alkali sorption at the silica-water surface is calculated as the difference between the initial and final dissolved sodium or cesium concentrations. Surface charge at the silica-water surface appears to be compensated by the uptake of the alkali ions with increasing pH to yield a neutral suspension. However, surface charge (or alkali sorption) cannot account for the dramatic decrease in silanol sites from pH 3 to 11 detected

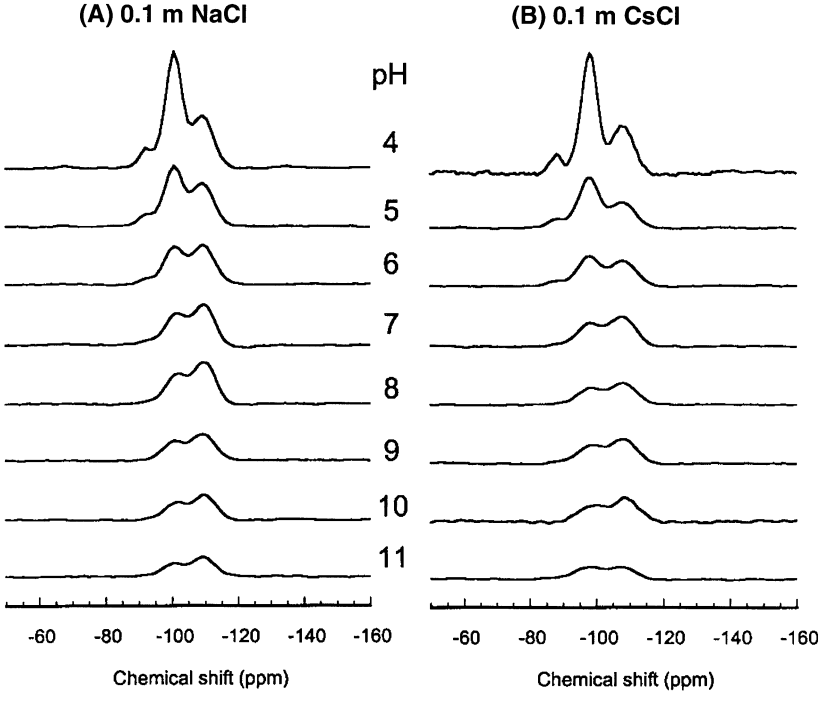

Fig. 4. The pH dependence of ^{29}Si cross-polarization magic-angle-spinning NMR spectra of amorphous silica reacted in 0.1-molal NaCl (A) and CsCl (B) solutions at 25°C. The spectra were recorded with identical acquisition parameters, normalized by weight and plotted relative to the same vertical scale. Spectra for experiments Si74 (pH 3.4), Si75 (pH 2.8), Si76 (pH4.0), are not shown because the spectra are identical to the pH4 spectra shown here.

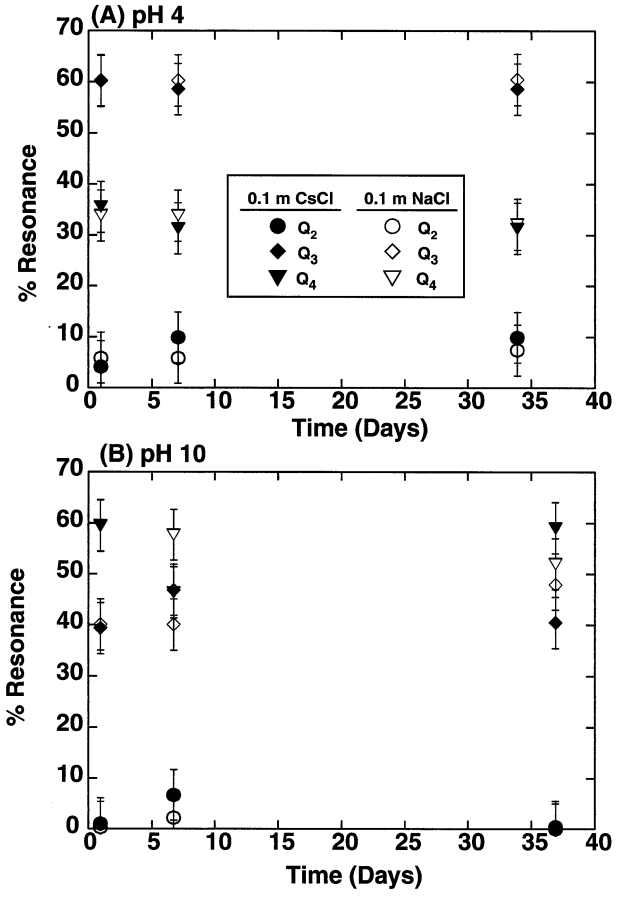

Fig. 5. Percentage of Q_2, Q_3, and Q_4 resonance for silica gel after 1, 7, and 30 d reaction in 0.1-molal NaCl or CsCl at pH 4 (A) and pH 10 (B). The speciation is reported as percent contribution to the total ^{29}Si cross-polarization spectrum based on gaussian fits of the Q_2, Q_3, and Q_4 resonances to the line shape. The percentages are not quantitative representations of species concentration.

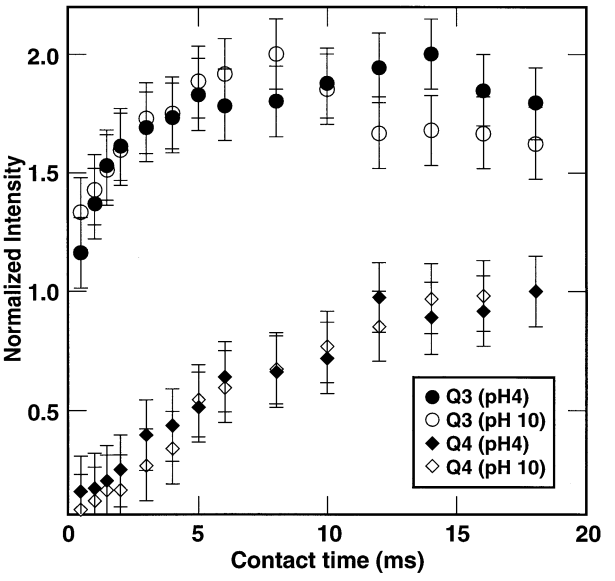

Fig. 6. The ^{29}Si cross-polarization resonance area versus cross-polarization contact time for silica gels reacted in pH 4 and pH 10 0.1-molal NaCl solutions at 25°C. The areas have been normalized by the maximum area of the specific resonance over the range of contact times. The areas for the Q_3 species have been vertically offset for clarity.

spectroscopically. This indicates that the silanol site must form a neutral complex that does not contribute to surface charge.

4. DISCUSSION

4.1. Surface Complexation Reactions at the Silica—Water Surface

Previous determinations of silica-water surface chemistry have been based on surface charge measured from acid-base titrations of silica suspensions. In these models the surface site density (N_T) is equal to:

$$N_T(mol\ m^{-2}) = \frac{([>SiOH] + [>SiO^-] + [>SiO^-M^+])}{A} \quad (5)$$

and the surface charge is equal to:

$$\sigma(C\ m^{-2}) = \frac{F}{A}(-[>SiO^-] - [>SiO^-M^+]) \quad (6)$$

where M^+ represents outersphere sorption of hydrated Na or Cs cations for our study. We use the $>SiO^-M^+$ notation for the outersphere complex because it shows the negative charge on the surface or *O*-plane and the positive charge of the hydrated cation in the β-plane proposed in Triple Layer Models (Yates et al., 1974; Davis et al., 1978). The concentration of >SiOH can be calculated from surface charge by combining Eqn. 5 and 6. Following this procedure, we observe a large discrepancy between >SiOH calculated from σ and >SiOH calculated from the NMR spectra (Fig. 7). In both cases we use a surface site density of 4.6 (site nm^{-2}). The cross-polarization ^{29}Si spectra show that the concentration of >SiOH complexes are strongly dependent on solution pH, such that they are ~80% lower at alkaline pH than calculated from models based on solution analyses alone (Eqn. 5 and 6).

A probable explanation for this discrepancy is the polymerization of silanol (Q_2 and Q_3) complexes with increasing pH. Mechanistically, polymerization is promoted by the deprotonation of >SiOH complexes to form siloxane bonds (>SiOSi<) at the silica-water surface, yielding a net reaction that does not generate or consume protons (Iler, 1979):

$$Deprotonation: >SiOH \Leftrightarrow >SiO^- + H^+ \quad (7)$$

$$Polymerization: >SiO^- + >SiOH \Leftrightarrow >SiOSi< + OH^- \quad (8)$$

$$Net\ Reaction: 2 > SiOH \Leftrightarrow >SiOSi< + H_2O \quad (9)$$

Thus polymerization accounts for the decrease in intensity of the silanol spectra without requiring an increase in surface charge (which is calculated from acid-base titration of the silica gel suspension). The extent of polymerization is the difference between >SiOH calculated from surface charge and >SiOH

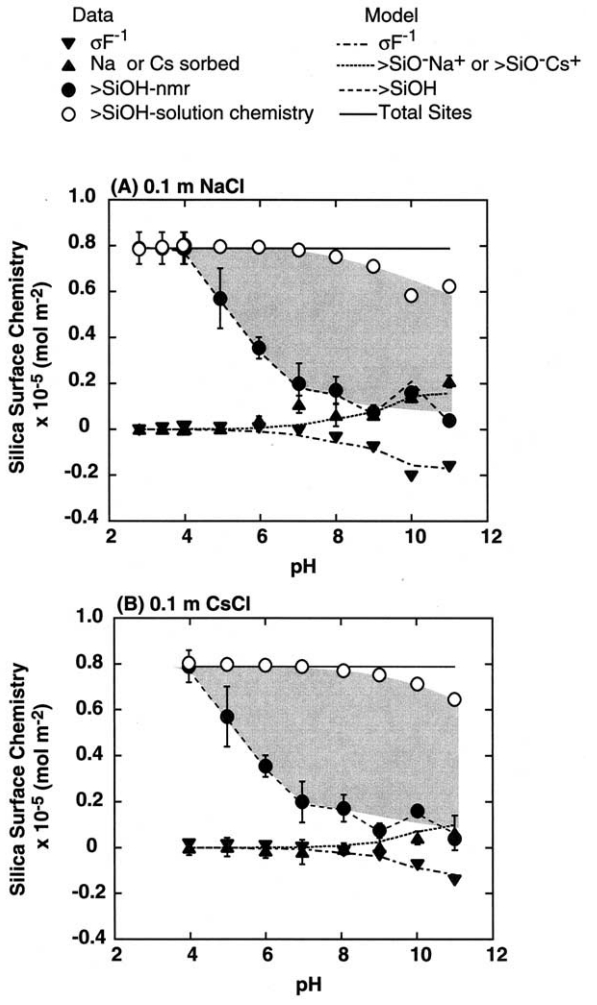

Fig. 7. Silica-water surface chemistry in 0.1-molal NaCl (A) and 0.1 molal CsCl solutions, as surface charge (σF^{-1}), total Na or Cs sorbed, >SiOH measured from the CPMAS ^{29}Si-NMR spectra, and >SiOH calculated from the solution chemistry. The shaded area highlights the difference between the concentration of >SiOH calculated from solution chemistry and from the NMR spectra, showing the number of >SiOH sites that polymerize to form >SiOSi<. The lines are triple layer surface complexation model fits to the data using the pH-dependent concentration of $>SiOH_{T,pH}$ sites derived from the NMR data (see text and Table 5).

calculated from the NMR spectra, and is highlighted as the shaded area in Figure 7.

We detect silica polymerization indirectly by the decrease in the intensity of the Q_2 and Q_3 spectra. We cannot measure polymerization directly as an increase in the Q_4 spectra, because the Q_4 spectra are the product of long range coupling between distal protons and fully polymerized silica at the surface and in the bulk solid. As such, the intensity of the Q_4 spectra depends on the intensity of the Q_2 and Q_3 spectra. Furthermore, surface polymerization would be difficult to detect, because it is estimated to comprise only 4 to 8% of bulk silica concentration, and is within the uncertainty of the NMR measurement. Although NMR has been used to study homogeneous polymerization in concentrated silica solutions (Kinrade, 1996; McCormick et al., 1988; Vega and Scherer, 1989), there are no studies that look at surface polymerization of simple silica gels. Polymerization of sodium-borosilicate glass surfaces using ^{17}O labeled water has been observed at acid pH, but not at alkaline pH (Bunker et al., 1988). This trend is opposite to our observations. However, one would not expect silica gel surface chemistry to be the same as a much more complex sodium-boro-silicate glass.

The observed increase in silica polymerization rates from solution and precipitation at the solid-solution interface indirectly support surface polymerization observed in this study. Silica polymerization from solution occurs at much faster rates above pH 2 (Iler, 1979). So much faster that silica polymerization kinetics from aqueous solutions are generally studied at acid pH, where the rate is slow enough to track the reaction. Heterogeneous precipitation rates of amorphous silica also increase slightly with increasing pH (Carroll et al., 1998).

Efforts to explicitly account for the polymerization reaction using surface complexation models failed, because polymerization is independent of solution pH (Eqn. 9) and predicts a constant >SiOSi< concentration (Fig. 7). This may indicate that a more complex surface complexation model is required. Or it may be an artifact that polymerization and precipitation reactions are not readily incorporated into FITEQL. However, if we directly solve for the concentration of $>SiOH_{T,pH}$ as a function of pH using the NMR data and the surface charge data ($[>SiOH]_{T,pH} = [SiOH]_{NMR} + \sigma F^{-1}$), then we get good agreement between the experimental data and the model predictions. We model our experimental data with the triple-layer surface complexation model, because it accounts for alkali sorption as outersphere complexes in agreement with the ^{23}Na and ^{133}Cs NMR spectroscopic observations. Table 5 lists the equilibria, mass balance, and charge balance equations used in our calculations. We do not consider the protonation reaction of the silanol sites, because they are believed to be negligible in the normal pH range, nor do we consider chloride sorption to protonated sites. The model fits to the data are shown in Figure 7. Surface complexation constants are log $K_{>SiO^-} = -7.5 \pm 1.0$, log $K_{>SiO-Cs+} = -7.77 \pm 0.08$, log $K_{>SiO-Na+} = -6.46 \pm 0.05$, and $C_1 = 1.0$ $C_2 = 0.2$ Fm^{-2}. With this model, the surface charge is mostly compensated by outersphere sorption of the alkali in the electrolyte solution. The amount of charge in the diffuse layer ranges from 10^{-6} molal at pH 4 to 10^{-3} molal at pH 11. These values are within the uncertainty of the charge balance of the aqueous solution of 2×10^{-3} molal (or 2% of electrolyte concentration).

4.2. pH Dependence of Silica Glass Dissolution Kinetics

At conditions far from equilibrium, surface chemistry appears to play a mechanistic role in amorphous silica reactivity as a function of pH. Regions of minimal dissolution rate are dominated by neutral >SiOH and >SiOSi< complexes, and regions of greater dissolution rate correlate with increasing concentration of the ionized surface complexes, $>SiO^-$ and $>SiO^-Na^+$ or $>SiO^-Cs^+$. This is shown by comparing the dependence of glass dissolution rates on pH (Fig. 1) and on the concentration of ionized surface complexes (Fig. 8). The correlation between dissolution rates and ionized surface complexes has been observed by other researchers, and implies that surface charge controls the vicinal structure of water and silica

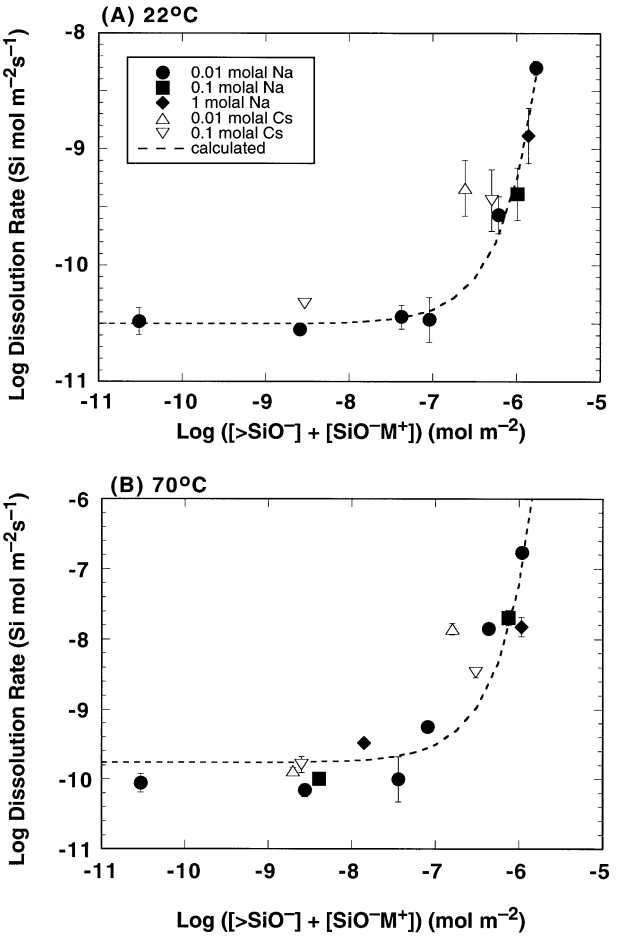

Fig. 8. SiO_2 glass dissolution rates in CsCl and NaCl solutions at 22°C (A) and 70°C (B) plotted as log dissolution rate Si (mol m^{-2} s^{-1}) versus log [SiO^-] + [SiO^-M^+] (mol m^{-2}). The dashed lines represent rates calculated from the overall rate expression (Eqn. 10).

hydrolysis for all silica polymorphs (Wirth and Gieskes, 1979; Fleming, 1986; Brady and Walther, 1990; Dove and Elston, 1992; Dove 1994). Within this framework, the primary reactants for silica dissolution are molecular water on a neutral surface and nucleophilic hydroxide on an ionized surface (Dove, 1994). Amorphous silica dissolution rates may be calculated as a function of total ionized sites, >SiO^- + >SiO^-Na^+, for the 0.01, 0.1, and 1 molal NaCl experiments at 22 and 70°C from the following empirical equation:

$$\log Rate(mol\ m^{-2}s^{-1}) = k_1 + k_2 \times ([>SiO^-] + [>SiO^-Na^+]) \quad (10)$$

where the temperature dependence of $k_1$and k_2 may be described by:

$$k_1 = -5.25 - \frac{29.7}{2.303RT} \quad (11)$$

and

$$k_2 = 1.06 \times 10^7 - \frac{5.30 \times 10^7}{2.303RT} \quad (12)$$

We use the experimental solution composition, a solid-to-solution ratio of 110 g L^{-1} (1 g glass and 9.1 mL solution), a surface area of 0.01 m^2 g^{-1}, and the $[SiOH]_{T,pH}$ and surface complexation constants determined from our silica gel experiments (0.1 molal) to calculate the glass surface chemistry over a range of salt concentrations (0.01 to 1 molal) and temperature (22 and 70°C). Application of the surface complexation model to the room temperature dissolution rates is straightforward and assumes that extent of polymerization and the pH dependence of the concentration of >SiOH is not dependent on ionic strength. To apply the room temperature surface complexation model to the 70°C dissolution rate data, we assume that the extent of polymerization, the pH dependence of >SiOH, the total site density, and interfacial capacitance constants are independent of temperature, and that the distributions of the surface complexes are controlled only by changes in aqueous dissociation constants with temperature. Thus, any systematic changes in surface chemistry with temperature are empirically accounted for in the temperature dependence of k_1 and k_2 in the rate expression (Eqn. 10). We did not include the dissolved silica concentrations in the analysis, because they were several orders of magnitude less than the total dissolved sodium concentrations and would not impact the surface speciation calculations. We plot the SiO_2 glass dissolution rates in CsCl solutions as a function of surface chemistry to compare to dissolution rates measured in the NaCl solutions, however no rate expression was developed because of a lack of data. The same protocol was used to calculate the glass surface chemistry in CsCl solutions as in NaCl solutions.

Comparison of Figures 1A and 8A, clearly show that the combined affects of pH and dissolved sodium on SiO_2 glass dissolution rates are best decribed in terms of the total concentration of ionized sites at the glass-solution interface at 22°C. The observed 0.5 log unit uncertainty in the dissolution rates from 0.01 to 1 molal sodium at about pH 9 in Figure 1A dissappear when the rates are plotted as a function of the glass surface chemistry in Figure 8A. At 70°C, the increased scatter in the dissolution rates as a function of surface chemistry most probably reflect our lack of knowledge of SiO_2 glass surface chemistry above room temperature (Fig. 8B). It appears that silica glass surface chemistry cannot be simply extrapolated from room temperature by assuming that surface chemistry is affected only by the temperature dependence of the aqueous dissociation constants. One would expect that glass dissolution rates in CsCl solutions would exhibit similar dependence on the concentration of ionized sites as it does in the NaCl solutions. Unfortunately, the scatter in the limited rate data at alkaline pH and 22°C is too large to see if this effect occurs, and at 70°C and alkaline pH, glass dissolution rate show an inverse relationship to the concentration of ionized sites in CsCl solutions. This observation, together with the negligible effect of the concentration of ionized sites at 70°C and alkaline pH in NaCl solutions, suggest that the nature of the alkali complex may change from outersphere at 22°C to innersphere at 70°C. The net effect of an innersphere alkalai complex would be to neutralize the surface and decrease the overall concentration of ionized sites. Additional experiments are needed to determine

important surface complexation reactions at elevated temperature.

4.3. Reaction Affinity

Reported decreases in silica polymorph dissolution and precipitation rates as dissolved silica concentrations approach saturation (Rimstidt and Barnes, 1980; Fleming, 1986; Renders et al., 1995; Carroll et al., 1998) appear to reflect the effects of solution composition rather than evolution of the silica surface chemistry. This observation suggests that the surface complexes represent reaction intermediates, and are not surrogates for activated complexes, because the silica dissolution rate is not stoichiometric with respect to changes in the concentration of the surface complexes. Specifically, we find no increase in polymerized surface complexes on the silica surface as identified by ^{29}Si cross-polarization magic-angle-spinning NMR spectroscopy with up to 30 d of reaction (Fig. 5) at pH 4 and pH 10. Over this same time period, net silica dissolution slowed as saturation was approached (Fig. 2). We would have expected to see a general decrease in the total ^{29}Si signal intensity Q_3 and Q_2 spectra, if polymerization at the surface controlled the decrease in dissolution rates with increased silica concentrations as equilibrium was approached. We do not think that the constant percentage of silanol complexes in the month long alkaline experiment is due to the drift from pH 10 to about pH 9, because their abundance in the one day experiments is within experimental error over this pH range. Note also that there was no drift in the pH 4 experiments. However, it is also possible that our inablity to detect the effects of saturation with the ^{29}Si-NMR data may be due to insufficient precipitation of ^{29}Si nuclei at the surface. A detailed investigation of the effects of solution saturation on dissolution mechanisms may require the use of isotopically labeled solutions.

5. CONCLUSIONS

Our research is motivated by the need to understand surface reactions dominating rock-water systems that are important to a wide variety of geochemical processes. Toward this end we have studied amorphous silica reactivity with flow-through dissolution and static batch experiments as a function of solution pH and reaction affinity. Our application of NMR spectroscopy to quantitatively measure in-situ surface speciation as a function of solution composition is new, and we have combined it with macroscopic solution analyses and surface complexation to describe the chemistry at the silica-water surface.

Our NMR results show that surface speciation is an equilibrium process, where changes in speciation are driven by solution pH and are not dependent on solution saturation. Surface polymerization, deprotonation, and alkali sorption are all dependent on solution pH. Surface polymerization was indirectly identified from the mismatch between the >SiOH concentration measured with ^{29}Si cross-polarization NMR spectroscopy and calculated from the acid-base chemistry alone. Our surface complexation model incorporates surface polymerization by directly accounting for the pH dependence of $>SiOH_{T,pH}$. Fits to the experimental data yield triple layer surface complexation constants of $\log K_{>SiO-} = -7.5 \pm 1.0$, $\log K_{>SiO-Cs+} = -7.77 \pm 0.08$, $\log K_{>SiO-Na+} = -6.46 \pm 0.05$, and capacitance constants $C_1 = 1.0$ and $C_2 = 0.2$ F m^{-2}. Development of surface charge is compensated by the sorption of alkali ions as outersphere complexes, as is indicated by the ^{133}Cs and ^{23}Na NMR spectra.

We use these surface complexation reactions to provide insight to the mechanisms controlling silica reactivity. In solutions far from amorphous silica saturation, the coupled dependence of silica glass dissolution rates on pH and sodium concentration may be correlated to concentration of ionized surface complexes. The catalytic effect of alkali ions on dissolution exceeds any inhibition due to the increase in surface polymerization with increasing pH. At conditions close to amorphous silica saturation, dissolution and precipitation reactions appear to be microscopically reversible. At constant pH, ^{29}Si cross-polarization, ^{23}Na and ^{133}Cs NMR data show the surface reactions are at equilibrium within 24 h and that no polymerization occurs at the interface as the solutions approach saturation with amorphous silica.

Acknowledgments—We thank B. Phillips for his contributions in the initial stages of our research, and we thank S. Roberts for assisting with the laboratory experiments. We also thank P. O'Day, K. Knauss and three anonymous reviewers for their helpful comments on an earlier version of this manuscript. This work was funded by the Department of Energy, Office of Basic Energy Science and performed under the auspices of the U.S. Department of Energy by Lawrence Livermore National Laboratory under Contract W-7405-ENG-48.

Associate editor: K. Ragnarsdottir

REFERENCES

Abragam A. (1961) Principles of Nuclear Magnetism. Oxford.

Allen L. H., Matijevic E., and Meites L. (1971) Exchange of Na^+ for the silanolic protons of silica. *J. Inorg. Nucl. Chem.* **33,** 1293–1299.

Ansermet J.-P., Slichter C. P., and Sinfelt J. H. (1990) Solid state NMR techniques for the study of surface phenomena. *Prog. NMR Spec.* **22,** 401–422.

Bennett P. C., Melcer M. E., Siegel C. I., and Hassett J. P. (1988) The dissolution of quartz in dilute aqueous solutions of organic acids at 25°C. *Geochim. Cosmochim. Acta.* **52,** 1521–1530.

Bennett P. C. (1991) Quartz dissolution in organic-rich aqueous systems. *Geochim. Cosmochim. Acta.* **55,** 1781–1798.

Berger G., Cadore E., Schott J., and Dove P. M. (1994) Dissolution rate of quartz in lead and sodium electrolyte solutions between 25 and 300°C: Effect of nature of surface complexes and reaction affinity. *Geochim. Cosmochim. Acta.* **58,** 541–552.

Bethke C. M. (1994) The geochemist's workbench. A user's guide to Rxn, Act2, Tact, React, and Gtplot. University of Illinois.

Bolt G. H. (1957) Determination of the charge density of silica sols. *J. Phys. Chem.* **61,** 1166–1169.

Brady P. V. and Walther J. V. (1989) Controls on silicate dissolution rates in neutral and basic pH solutions at 25°C. *Geochim. Cosmochim. Acta.* **53,** 2823–2830.

Brady P. V and Walther J. V. (1990) Kinetics of quartz dissolution at low temperatures. *Chem. Geol.* **82,** 253–264.

Brady P. V. (1992) Silica surface chemistry at elevated temperatures. *Geochim. Cosmochim. Acta.* **56,** 2941–2946.

Bronnimann C. E., Zeigler R. C., and Maciel G. E. (1988) Proton NMR study of dehydration of the silica gel surface. *J. Am. Chem. Soc.* **110,** 2023–2026.

Bunker B. C., Tallant D. R., Headley T. J., Turner G. L., and Kirkpatrick R. J. (1988) The structure of leached sodium borosilicate glass. *Phys. Chem. Glasses.* **29,** 106–120.

Carroll S. A., Bourcier W. L., and Phillips B. L. (1994) Surface chemistry and durability of borosilicate glass. *Mar. Res. Soc.* **333,** 533–540.

Carroll S. A., Mroczek E., Alai M., and Ebert M. (1998) Amorphous

silica precipitation (60 to 120°C): Comparison of laboratory and field rates. *Geochim. Cosmochim. Acta.* **62,** 1379–1396.

Casey W. H. (1994) Enthalpy changes for Bronsted acid-base reactions on silica. *J. Colloid Interface Sci.* **163,** 407–419.

Chuang I. S., Kinney, D. R., and Maciel G. E. (1993) Interior hydroxyls of the silica gel system as studied by Si-29 CP-MAS NMR spectroscopy. *J. Am. Chem. Soc.* **115,** 8695–8705.

Davis J. A., James R. O., and Leckie J. O. (1978) Surface ionization and complexation at the oxide/water interface I. Computation of electrical double layer properties in simple electrolytes. *J. Colloid. Interface Sci.* **63,** 480–499.

Davydov V. Y., Kiselev, A. V. and Zhuravlev L. T. (1964) Study of the surface and bulk hydroxyl groups of silica by infra-red spectra and D_2O-exchange. *Trans. Faraday Soc.* **60,** 2254–2264.

Dove P. M. and Crerar D. A. (1990) Kinetics of quartz dissolution in electrolyte solutions using a hydrothermal mixed flow reactor. *Geochim. Cosmochim. Acta.* **54,** 955–969.

Dove P. M. and Elston S. F. (1992) Dissolution kinetics of quartz in sodium chloride solutions: Analysis of existing data and a rate model for 25°C. *Geochim. Cosmochim. Acta.* **56,** 4147–4156.

Dove P. M. (1994) The dissolution kinetics of quartz in sodium chloride solutions at 25° to 300°C. *Am. J. Sci.* **294,** 665–712.

Dugger D. L., Stanton J. H., Irby B. N., McConnel B. L., Cummings W. W., and Maatman R. W. (1964) The exchange of twenty metal ions with the weakly acidic silanol group of silica gel. *J. Phys. Chem.* **68,** 757–760.

Fleming B. A. (1986) Kinetics of reaction between silicic acid and amorphous silica surfaces in NaCl solutions. *J. Coll. Interface Sci.* **110,** 40–64.

Fournier R. O. and Rowe J. J. (1977) The solubility of amorphous silica in water at high temperatures and high pressures. *Am. Mineral.* **62,** 1052–1056.

Herbelin A. L. and Westall, J. C. (1999) FITEQL: A computer program for determination of chemical equilibrium constants from experimental data. Oregon State University.

Hiemstra T., De Wit J. C. M., and Van Riemsdijk W. H. (1989) Multisite proton adsorption modeling at the solid/solution interface of (hydr)oxides: A new approach. II. Application to various important (hydr)oxides. *J. Colloid Interface Sci.* **133,** 105–117.

House W. A. and Orr D. R. (1992) Investigation of the pH dependence of the kinetics of quartz dissolution at 25°C. *J. Chem. Soc. Faraday Trans.* **88,** 233–241.

Iler R. K. (1979) The Chemistry of Silica. J. Wiley & Sons.

Johnson J. W., Oelkers E. H., and Helgeson H. C. (1992) SUPCRT92: A software package for calculating the standard molal thermodynamic properties of minerals, gases, aqueous species, and reactions from 1 to 5000 bar and 0 to 1000ºC. *Comp. Geosci.* **18,** 899–947.

Kim Y. and Kirkpatrick R. J. (1997) Na^{23} and Cs^{133} NMR study of cation adsorption on mineral surfaces: Local environments, dynamics, and effects of mixed cations. *Geochim. Cosmochim. Acta.* **61,** 5199–5208.

Kinrade, S. D. (1996) Oxygen-17 NMR study of aqueous potassium silicates. *J. Phys. Chem.* **100,** 4760–4764.

Kinrade S. D. and Swaddle T. W. (1988) Silicon-29 NMR studies of aqueous silicate solutions. 1. Chemical shifts and equilibria. *Inorg. Chem.* **27,** 4253–4259.

Knauss K. G. and Wolery T. J. (1986) Dependence of albite dissolution kinetics on pH and time at 25°C and 70°C. *Geochim. Cosmochim. Acta.* **50,** 2481–2497.

Knauss K. G. and Wolery T. J. (1988) The dissolution kinetics of quartz as a function of pH and time at 70°C. *Geochim. Cosmochim. Acta.* **52,** 43–55.

Liu C. C. and Maciel, G. E. (1996) The fumed silica surface: A study by NMR. *J. Am. Chem. Soc.* **118,** 5103–5119.

Maciel G. E. and Sindorf D. W. (1980) Silicon-29 nuclear magnetic resonance study of the surface of silica gel by cross polarization and magic-angle spinning. *J. Am. Chem. Soc.* **102,** 7606–7607.

Madeley J. D. and Richmond, R. C. (1972) A procedure for determining the concentration of hydroxyl groups on silica surfaces. *Z. Anorg. Allg. Chem.* **389,** 92–96.

Mazer J. J. and Walther J. V. (1994) Dissolution kinetics of silica glass as a function of pH between 40 and 85°C. *J. Non-Cryst. Sol.* **170,** 32–45.

McCormick A. V., Bell A. T., and Radke C. J. (1988) The effect of alkali metal cations on the structure of dissolved silicate oligomers. *Mat. Res. Soc.* **111,** 107–112.

Pines A., Gibby M. G., and Waugh J. S. (1973) Proton-enhanced NMR of dilute spins in solids. *J. Chem. Phys.* **59,** 569–590.

Renders P. J. N., Gammons C. H., and Barnes H. L. (1995) Precipitation and dissolution rate constants for cristobalite from 150 to 300°C. *Geochim. Cosmochim. Acta.* **59,** 77–85.

Rimstidt J. D. and Barnes H. L. (1980) The kinetics of silica-water reactions. *Geochim. Cosmochim. Acta.* **44,** 1683–1699.

Sahai N. and Sverjensky D. A. (1997) Evaluation of internally consistent parameters for the triple-layer model by the systematic analysis of oxide surface titration data. *Geochim. Cosmochim. Acta.* **61,** 2801–2826.

Schindler P. and Kamber H. R. (1968) Die Aciditat von Silanlogruppen. *Helv. Chim. Acta.* **51,** 1781–1786.

Schwartzentruber J., Furst W., and Renon H. (1987) Dissolution of quartz into dilute alkaline solutions at 90°C: A kinetic study. *Geochim. Cosmochim. Acta.* **51,** 1867–1874.

Tadros T. F. and Lyklema J. (1969) The electrical double layer on silica in the presence of bivalent counter-ions. *Electoranal. Chem. Interfac. Electrochem.* **22,** 1–7.

Vega A.J. and Scherer G. W. (1989) Study of structural evolution of silica gel using ^{1}H and. ^{29}Si NMR. *J. Non-Crystal. Sol.* **111,** 153–166.

Wijnen V. J. G., Beelen T. P. M., De Haan J. W., Van De Ven L. J. M., and Van Santen R. A. (1990) The structure directing effect of cations in aqueous silicate. *Coll. and Surf.* **45,** 255–268.

Wirth G. S. and Gieskes J. M. (1979) The initial kinetics of the dissolution of vitreous silica in aqueous media. *J. Col. Interf. Sci.* **68,** 492–500.

Wollast R. and Chou L. (1988) Rate control of weathering of silicate minerals at room temperature and pressure. In *Physical and Chemical Weathering in Geochemical Cycles* (eds. A. Lerman and M. Meybeck) 11–32.

Yates D. E., Levine, S., and Healy T. W. (1974) Site-binding model of the electrical double layer at the oxide/water interface. *J. Chem. Soc. Faraday Trans.* **70,** 1807–1818.

Yates D. E. and Healy T. W. (1976) The structure of the silica/electrolyte interface. *J. Col. Interf. Sci.* **55,** 9–19.

Zhuravlev L. T. and Kiselev A. V. (1962) Investigation of the hydroxyl layer of silica gel be deuterium exchange and adsorption of light and heavy water vapors. *Kolloidnyi Zhurnal.* **24,** 22–29.